Temperature Dependence of the Symmetry Energy in Finite Nuclei

M.K. Gaidarov[1], **A.N. Antonov**[1], **D.N. Kadrev**[1], **P. Sarriguren**[2], **E. Moya de Guerra**[3]

[1]Institute for Nuclear Research and Nuclear Energy, Bulgarian Academy of Sciences, Sofia 1784, Bulgaria

[2]Instituto de Estructura de la Materia, IEM-CSIC, Serrano 123, E-28006 Madrid, Spain

[3]Departamento de Fisica Atomica, Molecular y Nuclear, Facultad de Ciencias Fisicas, Universidad Complutense de Madrid, E-28040 Madrid, Spain

Abstract. The temperature dependence of the symmetry energy for isotopic chains of even-even Ni (A=58–82), Sn (A=124–152), and Pb (A=202–214) nuclei is investigated in the framework of the local density approximation. The Skyrme energy density functional with two Skyrme-class effective interactions, SkM* and SLy4, is used in the calculations. The temperature-dependent densities are calculated through the HFBTHO code that solves the nuclear Skyrme-Hartree-Fock-Bogoliubov problem by using the cylindrical transformed deformed harmonic-oscillator basis. In addition, two other density distributions of ^{208}Pb, namely the Fermi-type density determined within the extended Thomas-Fermi method and symmetrized-Fermi local density obtained within the rigorous density functional approach, are used. The results for the thermal evolution of the symmetry energy coefficient in the interval T=0–4 MeV show that its values decrease with temperature being larger in the case of the symmetrized-Fermi density of ^{208}Pb. It is observed that for all isotopic chains considered and for both Skyrme forces used in the calculations the symmetry energy coefficient decreases with the increase of the mass number in the same temperature interval.

1 Introduction

The nuclear symmetry energy is a measure of the energy gain in converting isospin asymmetric nuclear matter (ANM) to a symmetric system. Its value depends on the density ρ and temperature T. Experimentally, the nuclear symmetry energy is not a directly measurable quantity and is extracted indirectly from observables that are related to it [1]. The need of information for the symmetry energy in finite nuclei, even theoretically obtained, is a major issue because it allows one to constrain the bulk and surface properties of the nuclear energy-density functionals (EDFs) quite effectively. More information on the nuclear symmetry energy is still required for understanding the structures of

nuclei far away from the β-stability line, heavy-ion collisions, supernova explosions, and neutron star properties. A sensitive probe of the nuclear symmetry energy is the neutron-skin thickness of nuclei (see, for example, Ref. [2] and references therein) although its precise measurement is difficult to be done. As can be seen, e.g., in Refs. [3–7], an increasingly wide range of theoretical conclusions are being proposed on the density dependence of the symmetry energy as well as on some associated nuclear characteristics. In the last years, the temperature dependence of single-particle properties in nuclear and neutron matter was also broadly investigated including studies in finite systems, as well (e.g., Refs. [8–15]).

The thermal behavior of the symmetry energy has a role in changing the nuclear drip lines as the nuclei warm up. Also, it is of fundamental importance for the liquid-gas phase transition of asymmetric nuclear matter, the dynamical evolution mechanisms of massive stars and the supernova explosion [16]. Since the density derivative of the symmetry coefficient reflects the pressure difference on the neutrons and protons and thus it is one of the determinants in fixing the neutron skin of nuclei, the nature and stability of phases within a warm neutron star, its crustal composition or its thickness [17] would be strongly influenced by the temperature dependence of the symmetry energy.

In our previous works [18] and [19] the symmetry energy has been studied in a wide range of spherical and deformed nuclei, correspondingly, on the basis of the Brueckner EDF of ANM [20, 21]. In these works the transition from the properties of nuclear matter to those of finite nuclei has been made using the coherent density fluctuation model (CDFM) [22, 23]. In [18] the study of the correlation between the thickness of the neutron skin in finite nuclei and the nuclear symmetry energy (s) for the isotopic chains of even-even Ni (A=74–84), Sn (A=124–152) and Pb (A=206–214) nuclei, also the neutron pressure (p_0) and the asymmetric compressibility (ΔK) for these nuclei has been performed. The calculations have been based on the deformed self-consistent mean-field HF+BCS method using the CDFM and the Brueckner EDF. The same approaches have been used in Ref. [19] for the calculations of the mentioned quantities of deformed neutron-rich even-even nuclei, such as Kr (A=82–120) and Sm (A=140-156) isotopes. The numerical results for s, p_0, and ΔK for neutron-rich and neutron-deficient Mg isotopes with A=20–36 are presented in Ref. [24].

The main aim of this work is, apart from the ρ-dependence investigated in our previous works [18, 19, 24], to study also the temperature dependence of the symmetry energy in finite nuclei. We focus on the determination of the symmetry energy coefficient, for which we have explored the local density approximation (LDA) [10, 25] with some modifications. In the present paper the thermal evolution of the symmetry energy coefficient is investigated for Ni (A=58–82), Sn (A=124–152), and Pb (A=202–214) isotopic chains in the interval T=0–4 MeV using different model temperature-dependent local density distributions for these nuclei.

2 Theoretical Scheme

For finite systems, different definitions of the symmetry energy coefficient are adopted in the literature yielding different values. In our case we calculate the symmetry energy coefficient for a specific nucleus within the LDA and it is given as [10]

$$e_{sym}(A,T) = \frac{1}{I^2 A} \int \rho(r) e_{sym}[\rho(r), T] \delta_l^2(r) d^3 r. \tag{1}$$

In Eq. (1) $e_{sym}[\rho(r), T]$ is the symmetry energy coefficient at temperature T of infinite matter at the value of the local density $\rho(r)$, $\delta_l(r) = [\rho_n(r) - \rho_p(r)]/\rho(r)$ is the isospin asymmetry of the local density, where $\rho_n(r)$ and $\rho_p(r)$ are the neutron and proton densities, $\rho(r) = \rho_n(r) + \rho_p(r)$ and $I = (N - Z)/A$. The symmetry energy coefficient can be approximated by

$$e_{sym}(\rho, T) = \frac{e(\rho, \delta, T) - e(\rho, \delta = 0, T)}{\delta_l^2}, \tag{2}$$

where $e_{sym}(\rho, \delta, T)$ is the energy per nucleon in an asymmetric infinite matter, while $e(\rho, \delta = 0, T)$ is that one of symmetric nuclear matter. For an infinite system the energy per nucleon is calculated as $e = \varepsilon(r)/\rho$. We use for the total energy density of the system $\varepsilon(r)$ the Skyrme energy density functional with two Skyrme-class effective interactions, SkM* and SLy4. It is written as

$$
\begin{aligned}
\varepsilon(r) =\ & \frac{\hbar^2}{2m_{n,k}}\tau_n + \frac{\hbar^2}{2m_{p,k}}\tau_p \\
& + \frac{1}{2}t_0\left[\left(1 + \frac{1}{2}x_0\right)\rho^2 - \left(x_0 + \frac{1}{2}\right)(\rho_n^2 + \rho_p^2)\right] \\
& + \frac{1}{12}t_3\rho^\alpha\left[\left(1 + \frac{x_3}{2}\right)\rho^2 - \left(x_3 + \frac{1}{2}\right)(\rho_n^2 + \rho_p^2)\right] \\
& + \frac{1}{16}\left[3t_1\left(1 + \frac{1}{2}x_1\right) - t_2\left(1 + \frac{1}{2}x_2\right)\right](\nabla\rho)^2 \\
& - \frac{1}{16}\left[3t_1\left(x_1 + \frac{1}{2}\right) + t_2\left(x_2 + \frac{1}{2}\right)\right]\left[(\nabla\rho_n)^2 + (\nabla\rho_p)^2\right] \\
& + \varepsilon_c(r).
\end{aligned} \tag{3}
$$

In Eq. (3) t_0, t_1, t_2, t_3, x_0, x_1, x_2, x_3, and α are the Skyrme parameters (given in Table II of [10] for SkM* and SLy4 interactions). The nucleon effective mass $m_{q,k}$ is defined through

$$
\begin{aligned}
\frac{m}{m_{q,k}(r)} = 1 + \frac{m}{2\hbar^2}\Big\{&\left[t_1\left(1 + \frac{x_1}{2}\right) + t_2\left(1 + \frac{x_2}{2}\right)\right]\rho \\
& + \left[t_2\left(x_2 + \frac{1}{2}\right) - t_1\left(x_1 + \frac{1}{2}\right)\right]\rho_q\Big\},
\end{aligned} \tag{4}
$$

with $q = (n, p)$ referring to neutrons or protons. Here we would like to note that for infinite homogeneous systems only the first three lines of Eq. (3) contribute (the derivative terms are vanished) and the Coulomb term ε_c is neglected since the whole system is charge neutral.

In contrast to the methodology employed in Ref. [10], where the kinetic energy density $\tau_q(r)$ entering the expression for $\varepsilon(r)$ [Eq. (3)] is considered in the Thomas-Fermi approximation at finite temperature, we use in our theoretical scheme $\tau_q(r)$ from Ref. [13]

$$\tau_q(r) = \frac{2m}{\hbar^2}\varepsilon_{K_q} = \frac{3}{5}(3\pi^2)^{2/3}\left[\rho_q^{5/3} + \frac{5\pi^2 m_q^2}{3\hbar^4}\frac{1}{(3\pi^2)^{4/3}}\rho_q^{1/3}T^2\right], \quad (5)$$

which is valid at low T. The first term in square brackets is the degenerate limit at zero temperature and the T^2 term is the finite-temperature correction. By using the approximate expression (5) for the kinetic energy density, Lee and Mekjian performed calculations of the volume and surface symmetry energy coefficients for finite nuclei in Ref. [13] showing that the surface symmetry energy term is the most sensitive to the temperature while the bulk energy term is the least sensitive. The symmetry coefficient $e_{sym}(\rho, T)$ of ANM can then be computed from Eq. (2) and that one $e_{sym}(A, T)$ for finite nuclei from Eq. (1).

The temperature-dependent densities are calculated through the HFBTHO code that solves the nuclear Skyrme-Hartree-Fock-Bogoliubov (HFB) problem by using the cylindrical transformed deformed harmonic-oscillator basis [26] by implementing the finite temperature formalism for the HFB method. In addition, two other density distributions of ^{208}Pb [27], namely the Fermi-type density determined within the extended Thomas-Fermi (ETF) method [28] and the symmetrized-Fermi local density obtained within the rigorous density functional approach (RDFA) [29], are used. The density within the ETF method [28] which is the semi-classical limit of the temperature-dependent Hartree-Fock (THF) theory [30] has the form:

$$\rho_{ETF}(r, T) = \rho_0(T)\left\{1 + \exp\left[\frac{r - R(T)}{\alpha(T)}\right]\right\}^{-\gamma(T)}. \quad (6)$$

The temperature-dependent local density parameters ρ_0, R, α and γ are obtained for the nucleus ^{208}Pb with the SkM* effective force. The local densities (6) reproduce the averaged THF results up to temperature T=4 MeV [30]. The symmetrized-Fermi local density distribution determined for the same nucleus within the RDFA [29] is

$$\rho_{SF}(r, T) = \rho_0(T)\frac{\sinh[R(T)/b(T)]}{\cosh[R(T)/b(T)] + \cosh[r/b(T)]}. \quad (7)$$

The temperature-dependent local density parameters ρ_0, R, and b are obtained with the SkM effective force up to T=10 MeV. As has been demonstrated in [29],

65

the RDFA almost exactly reproduces the THF results [31] up to temperatures T=8 MeV above which the nucleus is unstable with respect to the THF calculations [31].

3   Results of Calculations and Discussion

We start our analysis by searching the role of temperature-dependent local density distributions $\rho(r)$ on the symmetry energy coefficient e_{sym}. The results for these densities of the nucleus ^{208}Pb obtained within different approaches
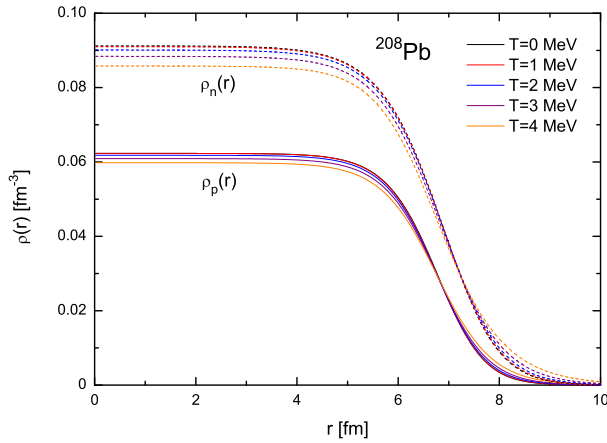

Figure 1. Proton and neutron local density distributions of ^{208}Pb obtained within the ETF method [28] and for temperatures $T = 0$–4 MeV.
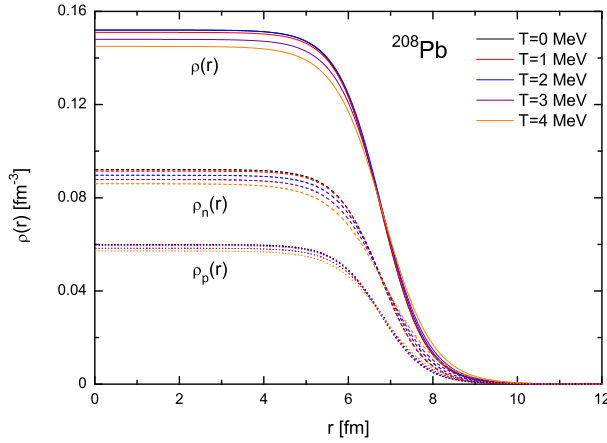
Figure 2. Proton, neutron and total local density distributions of ^{208}Pb obtained within the RDFA [29] and for temperatures $T = 0$–4 MeV.
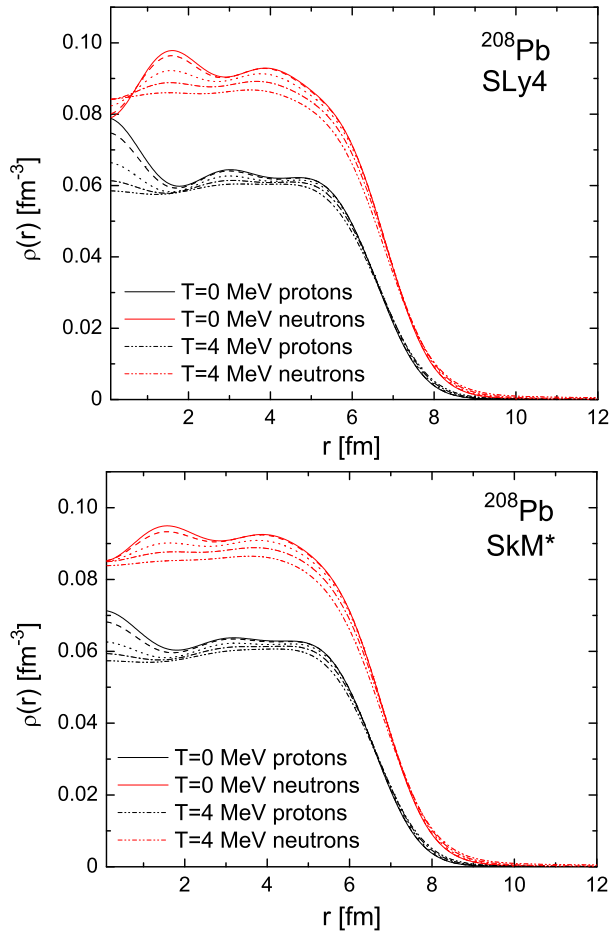
Figure 3. Proton and neutron local density distributions of ^{208}Pb obtained within the Skyrme HFB method [26] with SLy4 (top panel) and SkM* (bottom panel) forces. Five different curves for protons and neutrons represent the results for the corresponding densities for temperatures $T = 0$–4 MeV.

are given in Figures 1-3. In addition to the proton and neutron densities, normalized to Z=82 and N=126, respectively, that are presented in Figure 1, we give also in Figure 2 the total local density of ^{208}Pb normalized to A=208. It can be seen from both figures that ETF method and RDFA yield densities that have smooth behavior of r at any temperature T although the RDFA, in contrast to ETF method, incorporates the THF shell effects [27]. Figures 1 and 2 also show that with increase of the temperature the all type of densities decrease. This decrease is stronger for the neutron and total density distributions of ^{208}Pb. The proton and neutron local density distributions of ^{208}Pb obtained within the
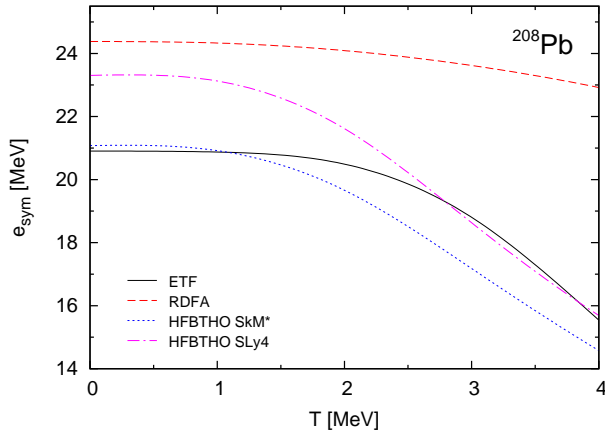
Figure 4. Comparison of the results for the symmetry energy coefficient e_{sym} for ^{208}Pb calculated with ETF, RDFA and HFB (with SkM* and SLy4 forces) densities.

Skyrme HFB method and illustrated in Figure 3 have somewhat different behavior. The same trend with the increase of the temperature can be observed, but in this case the local densities $\rho(r)$ exhibit a stronger T-dependence.

In understanding the symmetry energy coefficient e_{sym} for finite nuclear systems and their thermal evolution, some ambiguities about their proper definition could be noted. In our work we apply the LDA, in which the symmetry energy coefficient can be calculated by using Eq. (1). A comparison between the results for e_{sym} for ^{208}Pb with three different densities, namely obtained within the ETF, RDFA and HFB methods (with SkM* and SLy4 forces), is given in Figure 4. The results for the thermal evolution of the symmetry energy coefficient in the interval $T = 0$–4 MeV show that its values decrease with the temperature
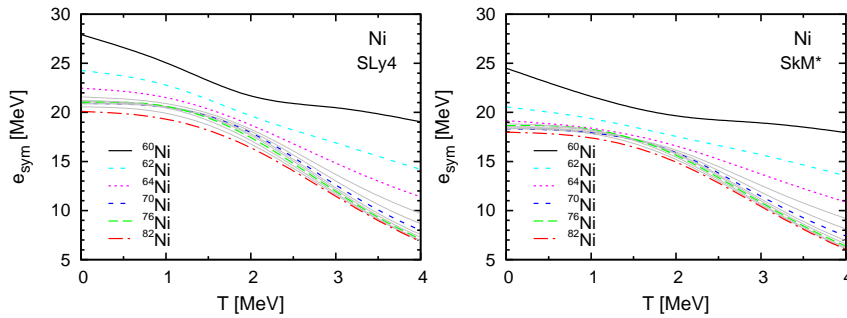

Figure 5. Temperature dependence of the symmetry energy coefficient e_{sym} obtained for several nuclei from Ni isotopic chain (A=60–82) in HFB method with SLy4 (left panel) and SkM* (right panel) forces.
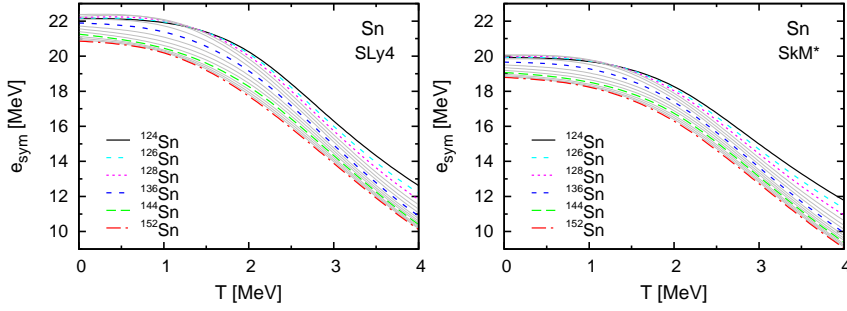
Figure 6. Temperature dependence of the symmetry energy coefficient e_{sym} obtained for several nuclei from Sn isotopic chain (A=124–152) in HFB method with SLy4 (left panel) and SkM* (right panel) forces.
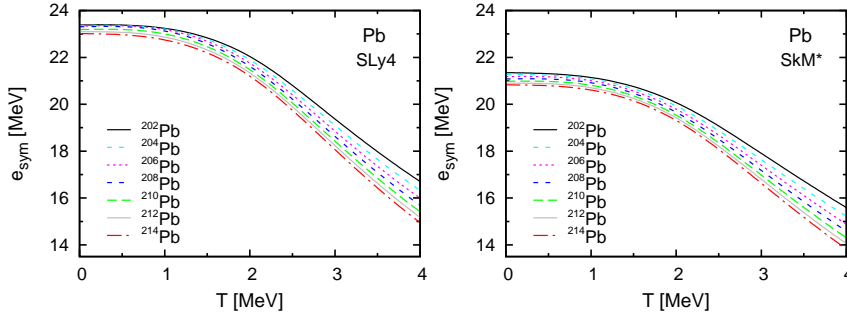

Figure 7. Temperature dependence of the symmetry energy coefficient e_{sym} obtained for several nuclei from Pb isotopic chain (A=202–214) in HFB method with SLy4 (left panel) and SkM* (right panel) forces.

being larger in the case of symmetrized-Fermi density of ^{208}Pb obtained within the RDFA. We would like to note that our results for e_{sym} are close to those obtained within the LDA in Ref. [10] for the same nucleus.

Figures 5–7 illustrate the isotopic evolution of the symmetry energy coefficient on the example of the Sn (A=124–152) and Pb (A=202–214) chains in the case of both SLy4 and SkM* Skyrme interactions used in the calculations. A smooth decrease of e_{sym} is observed with the increase of the mass number. We also would like to note the lack of kink for the Pb isotopic chain shown in Figure 7 when looking at the values of e_{sym} at zero temperature. This is not the case for the Ni and Sn isotopic chains (see Figures 5 and 6), where the order of the different curves at T=0 MeV exhibits a kink at the double-magic ^{78}Ni and ^{132}Sn nuclei. These results confirm our previous observations when studying the density dependence of the symmetry energy for Ni, Sn, and Pb isotopes [18,19].

4 Conclusions

The LDA is applied to study the temperature dependence of the symmetry energy coefficient. It is calculated for the nucleus ^{208}Pb using two types of temperature-dependent local density distributions within ETF method and RDFA. For the isotopic Ni, Sn, and Pb chains calculations are also performed with densities obtained in the framework of Skyrme HFB method by using the cylindrical transformed deformed harmonic-oscillator basis. For infinite ANM a Skyrme density functional with SkM* and SLy4 effective forces is used.

The ETF and RDFA results for the density distributions demonstrate a smooth function of r at any temperature T, while the Skyrme HFB densities have a stronger T-dependence. In general, the density distributions decrease with the temperature. The results for the thermal evolution of the symmetry energy coefficient in the interval T=0–4 MeV show that its values decrease with temperature being larger in the case of symmetrized-Fermi density of ^{208}Pb. It is observed that for all isotopic chains considered and for both Skyrme forces used in the calculations the symmetry energy coefficient decreases with the increase of the mass number in the same temperature interval.

Acknowledgements

References

[1] D.V. Shetty and S.J. Yennello, *Pramana* **75** (2010) 259-269.

[2] P. Sarriguren, M.K. Gaidarov, E. Moya de Guerra, and A.N. Antonov, *Phys. Rev. C* **76** (2007) 044322.

[3] Z.H. Li, U. Lombardo, H.-J. Schulze, W. Zuo, L.W. Chen, and H.R. Ma, *Phys. Rev. C* **74** (2006) 047304.

[4] J. Piekarewicz and M. Centelles, *Phys. Rev. C* **79** (2009) 054311.

[5] I. Vidaña, C. Providência, A. Polls, and A. Rios, *Phys. Rev. C* **80** (2009) 045806.

[6] F. Sammarruca and P. Liu, *Phys. Rev. C* **79** (2009) 057301.

[7] P. Danielewicz, arXiv:1003.4011 [nucl-th] (2010).

[8] Ch.C. Moustakidis, *Phys. Rev. C* **76** (2007) 025805.

[9] F. Sammarruca, arXiv:0908.1958 [nucl-th] (2009).

[10] B.K. Agrawal, J.N. De, S.K. Samaddar, M. Centelles, and X. Viñas, *Eur. Phys. J. A* **50** (2014) 19.

[11] B.K. Agrawal, D. Bandyopadhyay, J.N. De, and S.K. Samaddar, *Phys. Rev. C* **89** (2014) 044320.

[12] Z.W. Zhang, S.S. Bao, J.N. Hu, and H. Shen, *Phys. Rev. C* **90** (2014) 054302.

[13] S.J. Lee and A.Z. Mekjian, *Phys. Rev. C* **82** (2010) 064319.

[14] Bao-An Li and Lie-Wen Chen, *Phys. Rev. C* **74** (2006) 034610.

[15] A.Z. Mekjian, S.J. Lee, and L. Zamick, *Phys. Rev. C* **72** (2005) 044305.

[16] E. Baron, J. Cooperstein, and S. Kahana, *Phys. Rev. Lett.* **55** (1985) 126–129.

[17] A.W. Steiner, *Phys. Rev. C* **77** (2008) 035805.

[18] M.K. Gaidarov, A.N. Antonov, P. Sarriguren, and E. Moya de Guerra, *Phys. Rev. C* **84** (2011) 034316.

[19] M.K. Gaidarov, A.N. Antonov, P. Sarriguren, and E. Moya de Guerra, *Phys. Rev. C* **85** (2012) 064319.

[20] K.A. Brueckner, J.R. Buchler, S. Jorna, and R.J. Lombard, *Phys. Rev.* **171** (1968) 1188-1195.

[21] K.A. Brueckner, J.R. Buchler, R.C. Clark, and R.J. Lombard, *Phys. Rev.* **181** (1969) 1543-1551.

[22] A.N. Antonov, V.A. Nikolaev, and I.Zh. Petkov, *Bulg. J. Phys.* **6** (1979) 151; *Z. Phys. A* **297** (1980) 257; *ibid* **304** (1982) 239; *Nuovo Cimento A* **86** (1985) 23; A.N. Antonov *et al.*, *ibid* **102** (1989) 1701; A.N. Antonov, D.N. Kadrev, and P.E. Hodgson, *Phys. Rev. C* **50** (1994) 164-167.

[23] A.N. Antonov, P.E. Hodgson, and I.Zh. Petkov, *Nucleon Momentum and Density Distributions in Nuclei* (Clarendon Press, Oxford, 1988); *Nucleon Correlations in Nuclei* (Springer-Verlag, Berlin-Heidelberg-New York, 1993).

[24] M.K. Gaidarov, P. Sarriguren, A.N. Antonov, and E. Moya de Guerra, *Phys. Rev. C* **89** (2014) 064301.

[25] S.K. Samaddar, J.N. De, X. Viñas, and M. Centelles, *Phys. Rev. C* **76** (2007) 041602(R).

[26] M. Stoitsov, N. Schunck, M. Kortelainen, N. Michel, H. Nam, E. Olsen, J. Sarich, and S. Wild, *Comp. Phys. Commun.* **184** (2013) 1592–1604.

[27] A.N. Antonov, J. Kanev, I.Zh. Petkov, and M.V. Stoitsov, *Nuovo Cimento A* **101** (1989) 525-542.

[28] M. Brack, C. Guet, and H.-B. Håkansson, *Phys. Rep.* **123** (1985) 275-364.

[29] M.V. Stoitsov, I.Zh. Petkov, and E.S. Kryachko, *C. R. Bulg. Acad. Sci.* **40** (1987) 45; M.V. Stoitsov, *Nuovo Cimento A* **98** (1987) 725-744.

[30] M. Brack and P. Quentin, *Phys. Lett. B* **52** (1974) 159-162; *Phys. Scr. A* **10** (1974) 163-169; U. Mosel, P.G. Zint, and K.A. Passler, *Nucl. Phys. A* **236** (1974) 252-268.

[31] P. Bonche, S. Levit, and D. Vautherin, *Nucl. Phys. A* **427** (1984) 278-296; **436** (1985) 265-293.